

# Fast DAQ system with image rejection for axion dark matter searches

---

**S. Ahn,<sup>a,b</sup> M. J. Lee,<sup>b</sup> A. K. Yi,<sup>a,b</sup> B. Yeo,<sup>a,b,1</sup> B. R. Ko,<sup>b,2</sup> and Y. K. Semertzidis<sup>a,b</sup>**

<sup>a</sup>*Department of Physics, Korea Advanced Institute of Science and Technology (KAIST), Daejeon 34141, Republic of Korea*

<sup>b</sup>*Center for Axion and Precision Physics Research (CAPP), Institute for Basic Science (IBS), Daejeon 34051, Republic of Korea*

*E-mail:* [brko@ibs.re.kr](mailto:brko@ibs.re.kr)

**ABSTRACT:** A fast data acquisition (DAQ) system for axion dark matter searches utilizing a microwave resonant cavity, also known as axion haloscope searches, has been developed with a two-channel digitizer that can sample 16-bit amplitudes at rates up to 180 MSamples/s. First, we realized a practical DAQ efficiency of greater than 99% for a single DAQ channel, where the DAQ process includes the online fast Fourier transforms (FFTs). Using an IQ mixer and two parallel DAQ channels, we then also implemented a software-based image rejection without losing the DAQ efficiency. This work extends our continuing effort to improve the figure of merit in axion haloscope searches, the scanning rate.

---

<sup>1</sup>Now at Department of Physics, University of California, CA 94720, Berkeley, USA

<sup>2</sup>Corresponding author

---

## Contents

<b>1</b>	<b>Introduction</b>	<b>1</b>
<b>2</b>	<b>Fast digitizer</b>	<b>2</b>
2.1	Trigger	2
2.2	DAQ modes	3
2.2.1	STD mode	3
2.2.2	FIFO mode	3
2.3	Parameters	4
<b>3</b>	<b>Axion haloscope DAQ system</b>	<b>5</b>
<b>4</b>	<b>Single channel DAQ process</b>	<b>5</b>
4.1	Parallel data processing and sampling	5
4.2	Optimization of the DAQ cycle time segment	6
4.3	DAQ efficiency	7
4.4	Validation of the power fluctuations	8
<b>5</b>	<b>Image rejection DAQ system</b>	<b>11</b>
<b>6</b>	<b>Summary</b>	<b>11</b>

---

## 1 Introduction

A very natural solution to the strong  $CP$  problem in the Standard Model of particle physics (SM) [1] was proposed by Peccei and Quinn, who introduced a new global symmetry, PQ symmetry [2]. The breakdown of the PQ symmetry then results in the axion [3]. Provided the axion mass is light enough, above  $O(\mu\text{eV}/c^2)$  according to the original works [4] or above  $O(\text{peV}/c^2)$  by more recent works [5] and below  $O(\text{meV}/c^2)$  [6], the axion becomes one of the most promising candidates for cold dark matter (CDM). If the axion turns out to be 100% of CDM, the SM would be promoted as a model that would govern 31.7% of the total Universe energy budget, according to the precision cosmological measurements and the standard model of Big Bang cosmology [7].

The axion haloscope search by Sikivie [8] is the most sensitive axion dark matter search method to date. By employing a microwave resonant cavity, the axion signal power will resonate if the axion mass  $m_a$  matches the resonant frequency of the cavity mode  $\nu$ ,  $m_a = h\nu/c^2$ . Without knowing the axion mass, it is therefore obligatory for axion haloscope searches to be able to scan the resonant frequencies corresponding to possible axion masses. Accordingly, the scanning rate [9] for a target signal to noise ratio  $\text{SNR}_{\text{target}}$

$$\frac{d\nu}{dt} = \epsilon_{\text{DAQ}} \frac{\nu b_a}{Q_L} \left( \frac{\epsilon_{\text{SNR}}}{\text{SNR}_{\text{target}}} \right)^2 \left( \frac{P_a^{a\gamma\gamma}}{P_n} \right)^2 \propto \epsilon_{\text{DAQ}} \epsilon_{\text{SNR}}^2 \frac{g_{a\gamma\gamma}^4 B^4 V^2 C^2 Q_L}{\text{SNR}_{\text{target}}^2 T_n^2} \quad (1.1)$$

is usually referred to as the figure of merit in axion haloscope searches. In Eq. (1.1),  $P_a^{a\gamma\gamma}$  is the axion signal power proportional to  $g_{a\gamma\gamma}^2 B^2 V C Q_L$  [8, 9], where  $g_{a\gamma\gamma}$  is the axion-photon coupling strength,  $B$  is the static magnetic field provided by magnets in the axion haloscopes,  $V$  is the cavity volume,  $C$  is the form factor representing the overlap between the electric field of the cavity mode and the static magnetic field whose general definition can be found in Ref. [10], and  $Q_L$  is the loaded quality factor of the cavity mode.  $P_n$  is the noise power proportional to the noise temperature  $T_n$  and the axion signal window  $b_a$ .  $\epsilon_{\text{SNR}}$  is the reconstruction efficiency of the SNR in the axion haloscope search analysis procedures [11] and  $\epsilon_{\text{DAQ}}$  the DAQ efficiency. Although there was no explicit  $\epsilon_{\text{DAQ}}$  in Ref. [9] or in our previous publication [11], the DAQ efficiency is in practice very significant to the scanning rate, e.g., it was 47% with the spectrum analyzer R&S<sup>®</sup>FSV4 [12] in the CAPP-8TB experiment [13]. By doubling the  $\epsilon_{\text{DAQ}}$ , the speed of our axion haloscope searches will be boosted by a factor of two. In this work, we have realized a practical DAQ efficiency of greater than 99% using a fast digitizer, in a continuing effort following our previous study [11] to improve the scanning rate, where the DAQ process also includes online FFTs and writing the outputs to disk.

Axion haloscope searches generally employ a heterodyne receiver which introduces unwanted image backgrounds, thus could increase the background level about twice. With an image rejection of 30 dB, the background level would increase 0.1% which little affects the  $\text{SNR}_{\text{target}}$ , thus the scanning rate. The image rejection can be accomplished with a sharp bandpass filter [13], an image rejection mixer [14], or software utilizing in-phase (I) and quadrature (Q) signals from an IQ mixer [15]. We have implemented a software-based image rejection using an IQ mixer, and both DAQ channels on the digitizer. Without loss in  $\epsilon_{\text{DAQ}}$ , we have realized a fast DAQ system equipped with an image rejection of about 35 dB over a frequency range from 600 to 2200 MHz. Thus, it can be adopted by the CAPP-12TB axion dark matter experiment [16] which is expected to be sensitive to the Dine-Fischler-Srednicki-Zhitnitskii (DFSZ) axions [17] with help from other experimental parameters given in Sect. 4.4 and the DAQ parameters in Sect. 2.3.

## 2 Fast digitizer

The fast digitizer for this work is the M4i.4470-x8 from Spectrum Instrumentation GmbH [18]. The main features of the analog-to-digital converters (ADCs) are a 16-bit amplitude and a maximum sampling rate of 180 MSamples/s, where the former is responsible for the amplitude resolution and the latter for the time resolution, respectively. An external reference clock at 10 MHz has been used for the ADC operation. Two additional important capacities of the digitizer, an on-board memory of 2 GSamples and a transfer speed of  $\sim 3$  GB/s through the PCI Express x8 Gen2 interface, which can provide high efficiency on-board signal processing with proper DAQ parameters, enable this work.

### 2.1 Trigger

Since no specific events that could be detected as trigger events exist in the case of axion haloscope experiments, the trigger was activated forcibly or, equivalently, the trigger condition was set to be satisfied in all events.

## **2.2 DAQ modes**

Standard (STD) and First In, First Out (FIFO) are the two major options for the acquisition modes of the digitizer. Both modes include processes for allocating the buffer on the digitizer memory, sampling, and transferring the data on the digitizer memory to the PC memory. The difference between the two modes is about when and how the data are written and transferred to the buffers.

### **2.2.1 STD mode**

The STD mode process can be summarized as follows.

1. Define the total memory on the digitizer to be used.
2. Start the digitizer (acquisition) and force the trigger.
3. Wait until the acquisition is completed.
4. Define a buffer on the PC side (transfer buffer) for the data to be transferred into.
5. Transfer the data from the digitizer to the PC.

For our digitizer in this work, starting the digitizer is practically equivalent to starting the DAQ process. The acquisition of pretrigger data begins when the digitizer is started, and continued until the trigger is activated. After the trigger, the acquisition of posttrigger data is controlled by the digitizer, independently of system usage on the PC side. Completion of the acquisition can be recognized by writing a relevant register to the digitizer, which is released after all the data are acquired. This process is necessary in order to minimize the time gap between the end of the acquisition and the start of the data transfer. The data then can be transferred from the digitizer to the PC and post processing of the data can be performed.

### **2.2.2 FIFO mode**

The FIFO mode process is summarized next.

1. Define the total memory on the digitizer to be used.
2. Start the digitizer (acquisition) and force the trigger.
3. Define the transfer buffer.
4. Start the data transfer.
5. Wait until the particular size of the data (referred to as notify size) is acquired and transferred.
6. Loop the procedures 4 and 5 until the desired amount of data is acquired. Stop the acquisition and transfer explicitly with the user command.

In the FIFO mode, the data transfer can be started at any moment, even before the sampling has started, once the necessary buffers are defined. Since the data transfer speed is faster than the sampling rate, the data transfer can be done almost simultaneously with sampling, hence no additional waiting for data transfer is needed.

While the data transfers, an interrupt occurs each time the notify size of the data is transferred. After the interrupt, the transferred data can be post processed or saved to disk. Starting the post processing at each interrupt reduces the memory usage on the PC side significantly, particularly in the axion haloscope DAQ system, since at the end only the averaged spectrum in a particular frequency range will be saved as the final output. After that the acquisition and transfer can either be stopped, or continued for the next set of data. For the latter case it is necessary to release the space on the digitizer buffer occupied by the data already transferred, so that it can be used to write the new data when the buffer is full. This is particularly necessary when the total size of the data to be acquired is larger than the installed memory on the digitizer. For such procedures the buffer on the digitizer side is initially page-aligned, and the transfer buffer defined on the PC memory should be programmed to be page-aligned as well.

The choice of notify size is restricted to multiples of the operating system’s page size. Since the acquisition and transfer can only be stopped after the notify size of the data is transferred, there can be unnecessary additional sampling (oversampling) if the size of the desired number of samples is not divisible by the notify size. In practice, the additional time due to oversampling is negligible, since the total amount of data is usually significantly larger than the minimum notify size, while the maximum size of data in addition to what is required is less than the notify size. As an example, the total number of samples to be acquired is 225M for 10 seconds of sampling, with a sampling rate of 22.5 MSamples/s, while a typical minimum notify size is 4096 bytes, corresponding to 2048 samples. This results in at most 1664 additional samples, corresponding to 74  $\mu$ s of time.

### 2.3 Parameters

The typical intermediate frequency (IF) of 10.7 MHz can be chosen at the heterodyne receiver for the CAPP-12TB experiment. With a sampling rate of 22.5 MSamples/s, the Nyquist frequency is 11.25 MHz which can result in a power spectrum span of 1.1 MHz with the IF as the central frequency. The span of 1.1 MHz is much wider than the relevant CAPP-12TB parameters, cavity bandwidths of  $\sim$ 30 kHz and virtualized axion [19] signal windows of  $\sim$ 3 kHz, and thus meets the criteria of CAPP-12TB axion haloscope searches.

With a resolution bandwidth (RBW) of 20 Hz, data from this process can be used for nonvirtualized axions [20] whose signal windows are at most 20 Hz as well as virtualized axions mentioned above. This narrow RBW is also more effective for getting rid of IF and radio frequency (RF) interference as the narrow spikes in each power spectrum [21] of the virtualized axion dark matter searches that is what we are primarily after.

We chose a dynamic range of  $\pm$ 500 mV, which limits very high power electromagnetic interference backgrounds and provides a power resolution of about 0.5% with a 16-bit amplitude resolution of the digitizer and expected background power level of  $O(\mu$ W). Table 1 lists the digitizer parameters used in this work.

sampling rate	spectrum span	RBW	number of ADC data per power spectrum	dynamic range
22.5 MSamples/s	1.1 MHz	20 Hz	1125000	$\pm$ 500 mV

**Table 1.** Parameters for the digitizer.

### 3 Axion haloscope DAQ system

In general, the main data for axion haloscope searches consists of continuous RF signals resulting in power spectra at the end, where the power spectra can be acquired from online or offline FFTs. Online FFT can be done with a commercial spectrum analyzer. However, the rather low  $\epsilon_{\text{DAQ}}$  of 47% obtained with the spectrum analyzer R&S<sup>®</sup>FSV4 [12] in the CAPP-8TB experiment [13] mentioned above, resulted mainly from the online FFT of the spectrum analyzer. Although offline FFT can be realized with an extra conventional storage unit to save the ADC data for a chosen sampling rate of 22.5 MSamples/s in this work, here we will employ the online FFT as done in Ref. [15] using the full advantages of the digitizer, an on-board memory of 2 GSamples and a transfer speed of  $\sim 3$  GB/s. Our recent development of a field-programmable gate array realized a realtime DAQ system including the online FFT, albeit with a fixed RBW of 100 Hz and a power spectrum span of 500 kHz [22]. The DAQ system developed in this work is more flexible in the power spectrum parameters, RBW and span, in addition to the image rejection using two parallel DAQ channels.

## 4 Single channel DAQ process

### 4.1 Parallel data processing and sampling

The challenging part of our DAQ system using the fast digitizer is the post processing of the data, which includes unit conversion, online FFT, averaging, and writing the power spectra (ROOT [23] format in this work) to disk storage. The online FFT dominates the post processing time. In most cases axion haloscope experiments require data at different resonance frequencies, because the axion mass is unknown. Also for various reasons the data at each resonance frequency can be divided into several subsets at different timestamps. In such cases, the post process can be performed in parallel while the next data is sampled. Python's multiprocessing module [24] was used to demonstrate such a scenario.

The essential parts of the post processing including writing to disk are defined separately, then integrated into a single function. The function is then called in a child process spawned by the main process at the end of the first DAQ cycle. The DAQ cycle ends as the child process starts, and the main process controls the digitizer to start a new DAQ cycle while the child process is running. After the new process ends the main process lets the child process join, then spawns more child processes for post processing the data from the new DAQ cycle. These procedures are repeated until the last DAQ cycle, and the main process ends before the post processing of data from the last DAQ cycle starts. For the detailed  $\epsilon_{\text{DAQ}}$  studies given in Sect. 4.3, the main process ends after the post processing of data from the last DAQ cycle ends.

In the child process, the data arrays are, at first, converted into a two dimensional array with each row containing a single spectrum. Then two child processes are again spawned, one for FFT and the other one for averaging the spectra and saving into a file. During the FFT process the data in each row are converted into voltage, and Fourier transformed. The output of the FFT is normalized and then converted into a single power spectrum. The power spectrum is finally put into a queue defined globally at the beginning of the main process. The other process receives the power spectra from the queue whenever it is filled, adds them together in a new buffer, divides it by the number

of spectra after the last power spectrum is added, then saves it in the data file. Finally the two child processes merge with their parent processes, and again merge with the main process.

The main process waits until the child process from a previous DAQ cycle merges with its parents. This means the next DAQ cycle might be delayed if the total time necessary for the post process exceeds the DAQ cycle time segment explained below. The total time for post processing can be reduced in this case by employing several parallel jobs in multi-thread CPUs.

With multi-thread CPUs, each FFT process can be shortened by multi-threading, or the overall tasks can be divided and done by several threads in parallel. Considering the large number of iterations and the fairly short time for each iteration, the latter is in practice more efficient. Since the FFT processes are already being performed in parallel and automatically assigned to another thread, using more threads can be done simply by dividing the tasks equally and spawning more FFT processes for assigning the divided tasks. Figure 1 shows the schematic of our DAQ process described above.

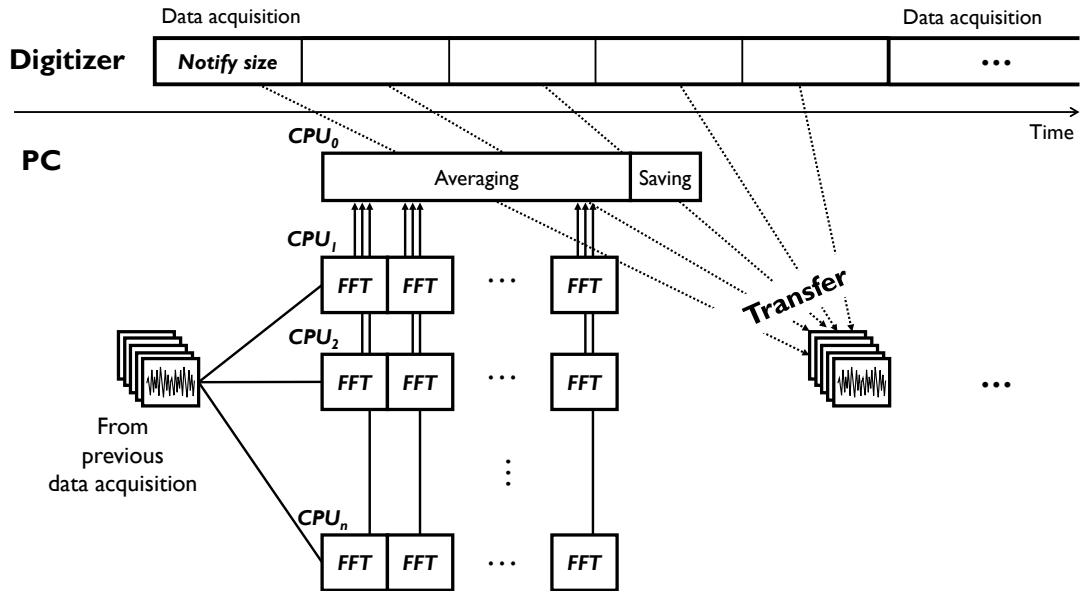
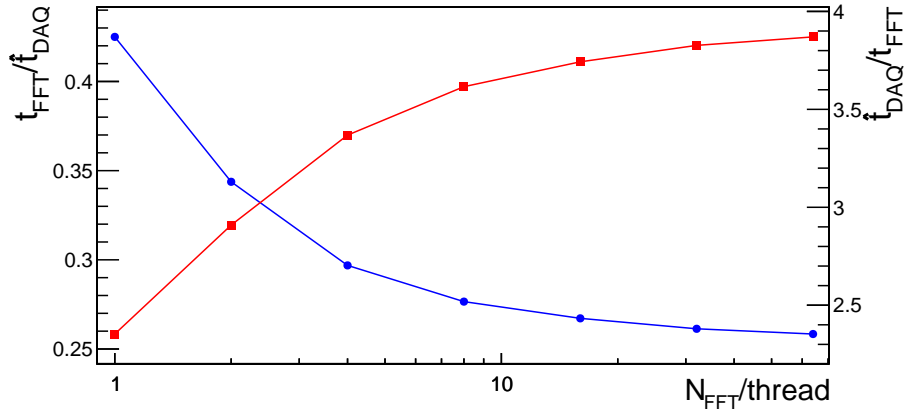


Figure 1. Schematic of the DAQ process.

## 4.2 Optimization of the DAQ cycle time segment

Here we address how the DAQ cycle time segment was optimized with our DAQ PC which has a 16-thread CPU whose maximum clock speed is 5.3 GHz according to the manufacturer [25]. We found the optimum cycle time by varying the number of FFTs or, equivalently, the number of power spectra, per thread. Figure 2 shows that a time ratio of FFT to DAQ cycle below 30% can be obtained by choosing the number of FFTs per thread to be greater or equal to 4. Our choice of the number of FFTs per thread was 8. From 128 FFTs (or power spectra) with 16 threads, therefore, our DAQ cycle time segment  $\hat{t}_{\text{DAQ}}$  was 6.4 s, corresponding to a data size of 288 MB for a single channel.



**Figure 2.** Time ratio of FFT to DAQ cycle (blue circles) and its reciprocal (red rectangles) as a function of number of FFTs per thread with the STD mode, where the latter can be read as the speedup depending on the parallel portion for a given number of threads [26].

### 4.3 DAQ efficiency

From the radiometer equation [27], the experimentally achieved SNR with an  $\epsilon_{\text{SNR}}$  of 100% [11] is

$$\text{SNR}_{\text{achieved}} = \frac{P_a^{a\gamma\gamma}}{\sigma_{P_n}} = \frac{P_a^{a\gamma\gamma}}{P_n} \sqrt{b_a t_{\text{DAQ}}} = \frac{P_a^{a\gamma\gamma}}{P_n} \sqrt{N}, \quad (4.1)$$

where  $\sigma_{P_n}$  is the  $P_n$  fluctuation,  $t_{\text{DAQ}}$  is the DAQ cycle time, and  $N$  is the number of power spectra, which shows that the axion dark matter search sensitivity can be improved by increasing the DAQ cycle time or, equivalently, the number of power spectra, by increasing the number of DAQ cycles. Therefore,  $t_{\text{DAQ}}$  is equal to  $n_{\text{iter}} \hat{t}_{\text{DAQ}}$  and our  $\epsilon_{\text{DAQ}}$  depends on  $n_{\text{iter}}$  with our DAQ algorithm explained above, where  $n_{\text{iter}}$  is the number of iterations for each resonant frequency scan. In our DAQ algorithm developed in this work, the first iteration time includes the digitizer starting ( $t_{\text{digitizer starting}}$ ) and DAQ cycle, while the second includes the next DAQ cycle and online FFTs with ADC data from the first iteration, where online FFTs are executed in parallel with the current DAQ cycle. Subsequent iterations are identical to the second iteration, until the last iteration which is like the second one except for the additional online FFTs using ADC data from the iteration ( $t_{\text{last FFTs}}$ ). Therefore, the DAQ efficiencies of the first and last iterations are lower because of the digitizer starting and the last online FFTs, respectively. The two inefficiency sources, however, become negligible as the  $n_{\text{iter}}$  increases. Even without the  $n_{\text{iter}}$  increasing, the inefficiency from the last online FFTs can be in practice ignored because the next resonant frequency scan can start right after the final iteration of data sampling, and the corresponding online FFTs can be finished during the cavity tuning and measurements before starting the new DAQ process.

The timestamp of the digitizer has limited usage, but turns out to be consistent with that of DAQ PC as shown in Fig. 3. This enables us to use handy timestamps from the PC. With an  $n_{\text{iter}}$  of 10000 and the STD mode, Table 2 shows the  $\epsilon_{\text{DAQ}}$  depending on the conditions, and Fig. 4 shows the distribution of the timestamp differences between two consecutive iterations  $\Delta t$ . As mentioned above,  $\epsilon_{\text{DAQ}}$  with a large enough  $n_{\text{iter}}$  is independent of the two significantly inefficient iterations shown in Fig. 4. Figure 5 shows the DAQ efficiency as a function of the number of iterations for



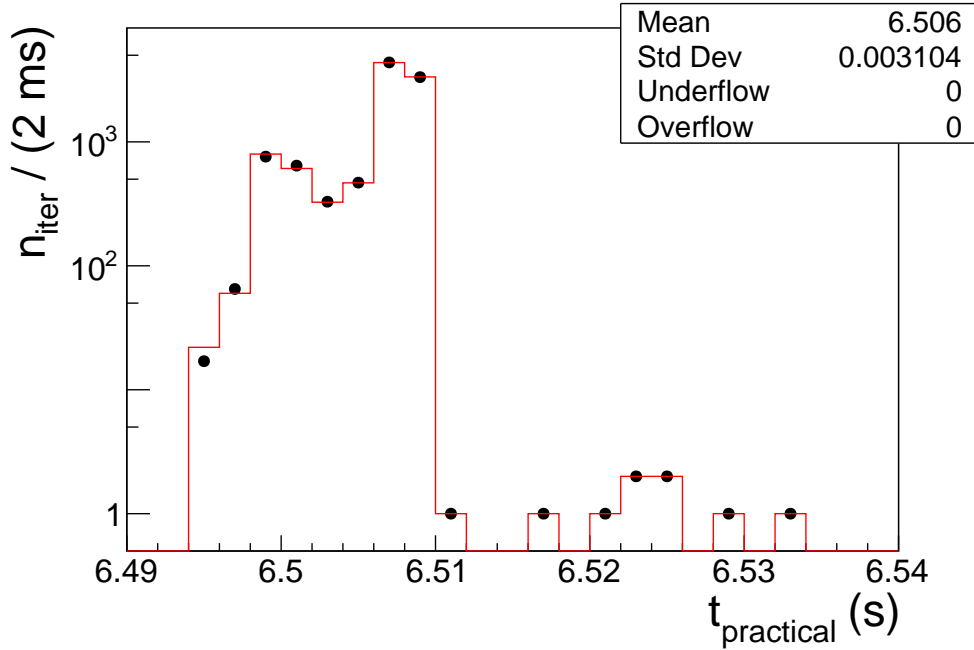


**Figure 3.** Timestamps from the digitizer (black circular markers) and DAQ PC (red histogram) with the STD mode.  $t_{\text{practical}}$  is equal to  $t_{\text{total}} - t_{\text{last FFTs}} - t_{\text{digitizer starting}}$  and used to estimate the  $\epsilon_{\text{DAQ}}$  with a practical number of iterations for a targeted experimental sensitivity.  $t_{\text{total}}$  is the total time including  $t_{\text{digitizer starting}}$  and  $t_{\text{last FFTs}}$  from the first and last iterations, respectively, as well as  $t_{\text{DAQ}}$ , where  $t_{\text{digitizer starting}}$  and  $t_{\text{last FFTs}}$  are explained the text above.

$\epsilon_{\text{DAQ}}$ with $n_{\text{iter}} = 10000$	conditions
$\frac{t_{\text{DAQ}}}{t_{\text{total}}} = 98.37\%$	with the last FFTs ( $t_{\text{last FFTs}}$ ) and digitizer starting
$\frac{t_{\text{DAQ}}}{t_{\text{total}} - t_{\text{last FFTs}}} = 98.38\%$	with the digitizer starting ( $t_{\text{digitizer starting}}$ )
$\frac{t_{\text{DAQ}}}{t_{\text{total}} - t_{\text{last FFTs}} - t_{\text{digitizer starting}}} = 98.39\%$	practical or, equivalently, without $t_{\text{last FFTs}}$ and $t_{\text{digitizer starting}}$

**Table 2.**  $\epsilon_{\text{DAQ}}$  of the STD mode with  $n_{\text{iter}}$  of 10000 depending on the conditions given in the second column.

both the STD and FIFO modes of the digitizer. The efficiencies are already higher than 98% and 99% after  $\sim 200$  iterations ( $N$  of  $\sim 26000$ ) or  $\sim 22$  minutes for the STD and FIFO modes, respectively, and then converge to 98.4% and 99.7% with further iterations.

#### 4.4 Validation of the power fluctuations

We checked whether the noise power fluctuations from our data with the DAQ process follow Eq. (4.1) using a  $50 \Omega$  termination input, where the fluctuations are the axion haloscope resolutions when they are measured through a full signal chain, i.e., a cavity, preamps, and digitizer or spectrum analyzer at the end. Figure 6 shows the noise power fluctuations depending on the number of power spectra, and they show good agreement with Eq. (4.1) as it should be, which is a fundamental requirement of the DAQ system for axion dark matter searches. Table 3 shows the expected CAPP-12TB experimental parameters for the resonant frequency  $\nu = 1$  GHz, where the coupling strength

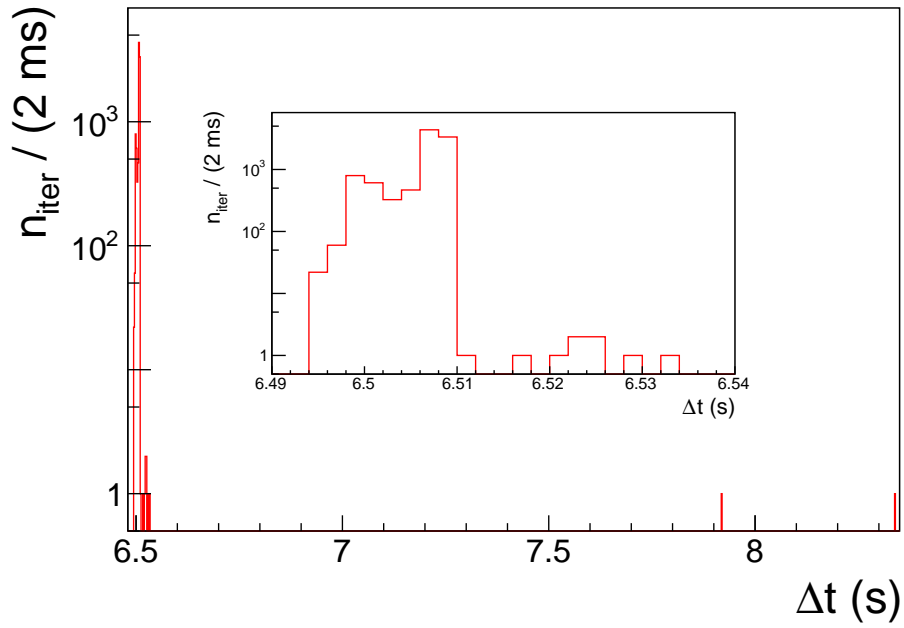


**Figure 4.** Distribution of  $\Delta t$  with the STD mode, where the inset shows that  $\Delta t$  around 6.5 s and is equivalent to the histogram in Fig. 3. Two entries  $\Delta t$  around 7.9 and 8.3 s correspond to the first and last iterations, respectively.

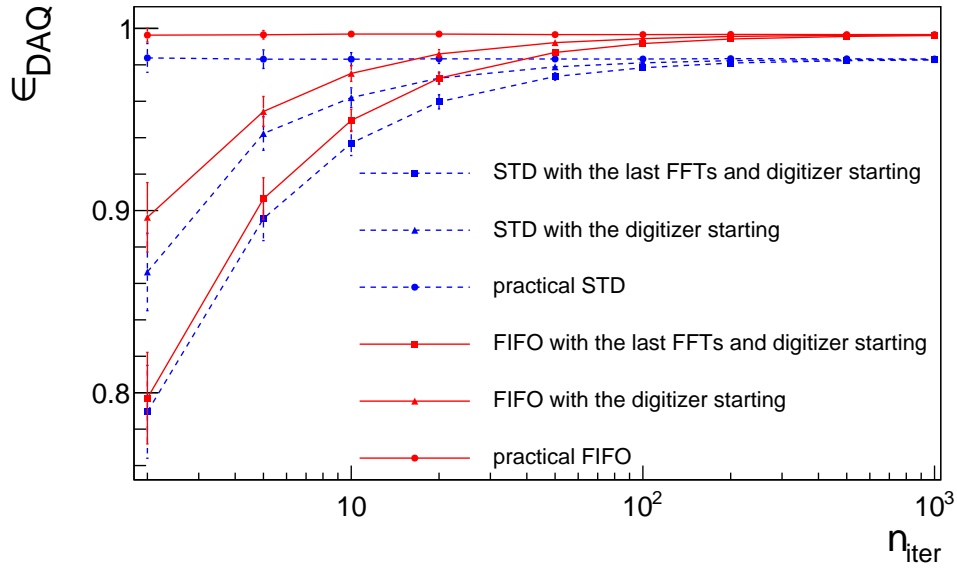


**Figure 5.** DAQ efficiencies with the binomial errors as a function of the number of iterations. The blue dashed lines (red solid lines) with rectangles, triangles, and circles show the efficiencies employing the STD (FIFO) mode depending on the conditions listed in Table 2, respectively.

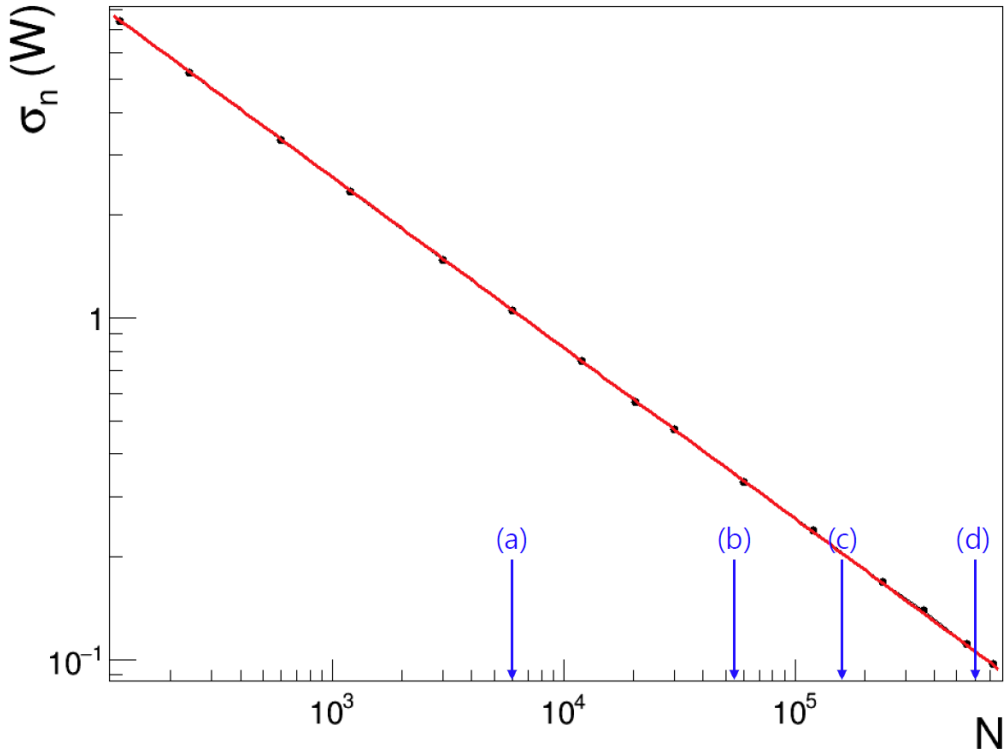


**Figure 6.** Noise power fluctuation  $\sigma_n$  with an arbitrary normalization as a function of the number of power spectra  $N$ , where the dots (black) are the measurements and line (red) is the expected from Eq. (4.1). The arrows (a), (b), (c), and (d) indicate the numbers of power spectra to meet an  $\text{SNR}_{\text{achieved}}$  of 5 for  $T_n$  of 0.1, 0.3, 0.5 and 1 K, respectively, for the  $g_{a\gamma\gamma}$  in Table 3.

$g_{a\gamma\gamma}$  corresponds to the DFSZ axion and  $\beta$  denotes the cavity mode coupling to the load. Given the

$g_{a\gamma\gamma}$	$B$	$V$	$C$	$Q_L$	$\beta$	$\nu$	$b_a$
$5.64 \times 10^{-16} \text{ GeV}^{-1}$	10.85 T	30 L	0.56	35000	2	1 GHz	3200 Hz

**Table 3.** Expected CAPP-12TB experimental parameters for the resonant frequency  $\nu = 1$  GHz. The coupling  $g_{a\gamma\gamma}$  is given in natural units.

experimental parameters listed in Table 3, Fig. 6 also shows the necessary number of power spectra to be sensitive to an  $\text{SNR}_{\text{achieved}}$  of 5 for the DFSZ axions, depending on the noise temperature. Accordingly, the DAQ efficiencies ignoring the last FFTs are higher than 99.2% with a noise temperature higher than 0.1 K in the FIFO mode. This noise power fluctuation study validates that the data from this DAQ process can be sensitive to the DFSZ axion even with a noise temperature of 1 K, if it goes with the CAPP-12TB experiment. Note that the statistics for this validation study was set to match the CAPP-12TB experiment, but the validation of our DAQ process can be extended easily to other experiments depending on the experimental parameters.

## 5 Image rejection DAQ system

Equation (5.1) shows the RF signals that contribute to the IF signals in typical axion haloscope searches employing a heterodyne receiver, where the first term on the right-hand side is the signal  $s(t)$  at  $f_{\text{RF}}$  and the second is the image background  $b(t)$  at  $f_{\text{IM}}$ .

$$v_{\text{RF}}(t) = s(t) \cos(\omega_{\text{RF}}t + \phi) + b(t) \cos(\omega_{\text{IM}}t + \phi), \quad (5.1)$$

where  $\omega = 2\pi f$  and  $\phi$  is a phase. Adopting  $\omega_{\text{IF}} = \omega_{\text{RF}} - \omega_{\text{LO}}$ , then  $\omega_{\text{IM}} = \omega_{\text{RF}} - 2\omega_{\text{IF}}$ , where LO stands for a local oscillator.

Downconverting  $v_{\text{RF}}(t)$  using an RF mixer and signal generator as an LO results in the IF signals expressed by Eq. (5.2).

$$v_{\text{IF}}(t) = \frac{a_{\text{LO}}}{2} (s(t) \cos(\omega_{\text{IF}}t + \phi) + b(t) \cos(\omega_{\text{IF}}t - \phi)), \quad (5.2)$$

where  $a_{\text{LO}}$  is the LO amplitude and the second term on the right-hand side is the unwanted image background at  $f_{\text{IF}}$ , which can be rejected by hardware [13, 14] or software [15]. In this work, we employed a software-based image rejection using a PolyPhase IQ mixer QD0622B [28], and both DAQ channels on the digitizer.  $V_{\text{IF}}^{\text{I}}(f)$  and  $V_{\text{IF}}^{\text{Q}}(f)$  are the complex FFT outputs of the ADC data from the I and Q channels of the mixer, respectively. One, then, can reject the image background by constructing Eq. (5.3) with real and imaginary parts of  $V_{\text{IF}}^{\text{I}}(f)$  and  $V_{\text{IF}}^{\text{Q}}(f)$ .

$$V_{\text{IF}}(f) = (\Re(V_{\text{IF}}^{\text{I}}(f)) + \Im(V_{\text{IF}}^{\text{Q}}(f))) + i(\Im(V_{\text{IF}}^{\text{I}}(f)) - \Re(V_{\text{IF}}^{\text{Q}}(f))). \quad (5.3)$$

The image rejection using Eq. (5.3) was measured over a frequency range from 600 to 2200 MHz and Fig. 7 shows the results  $\frac{P_{\text{input}}}{P_{\text{output}}}$  in dB as a function of the RF frequency, where  $P_{\text{input}}$  was set to 0 dBm. Note that  $P_{\text{input}}$  were injected to  $f_{\text{IM}} = f_{\text{RF}} - 2f_{\text{IF}}$  and  $P_{\text{output}}$  were measured at  $f_{\text{IF}} = 10.7$  MHz. Without losing the  $\epsilon_{\text{DAQ}}$  practically, as shown in Fig. 8, we realized a fast DAQ system equipped with an image rejection of about 35 dB over a frequency range from 600 to 2200 MHz. Note, however, that the image rejection here can go to any frequency with the relevant IQ mixers.

## 6 Summary

A DAQ system using a two-channel fast digitizer that can sample 16-bit amplitudes at rates up to 180 MSamples/s was developed to improve the figure of merit in axion haloscope searches, the scanning rate. The achieved DAQ efficiency, including the online FFT and writing the outputs to disk, is practically 100%, which is a significant improvement compared with our previous DAQ system using a commercial spectrum analyzer [13]. The limits of  $g_{a\gamma\gamma}$  from the CAPP-8TB experiment [29] can be improved from about  $1.00 \times 10^{-14}$  to  $0.83 \times 10^{-14}$   $\text{GeV}^{-1}$  by running the same experimental period employing the DAQ system in this work and can reach  $0.79 \times 10^{-14}$   $\text{GeV}^{-1}$  by putting our previous improvement [11] together.

Using the two channels on the digitizer and an IQ mixer, our DAQ system also has an image rejection of about 35 dB over a frequency range from 600 and 2200 MHz, without losing the DAQ efficiency practically, e.g., for the CAPP-12TB experiment [16]. This means the DAQ system developed in this work shows various improvements that allow the CAPP-12TB axion dark matter experiment to be sensitive the DFSZ axions in relevant frequency ranges.

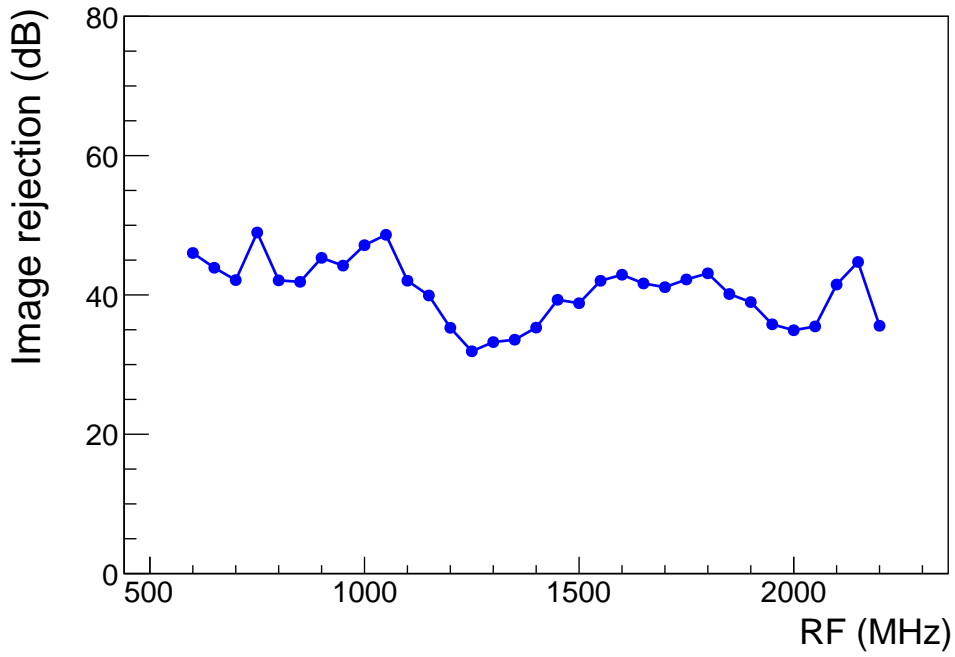


**Figure 7.** Image rejection in dB as a function of the RF frequency.

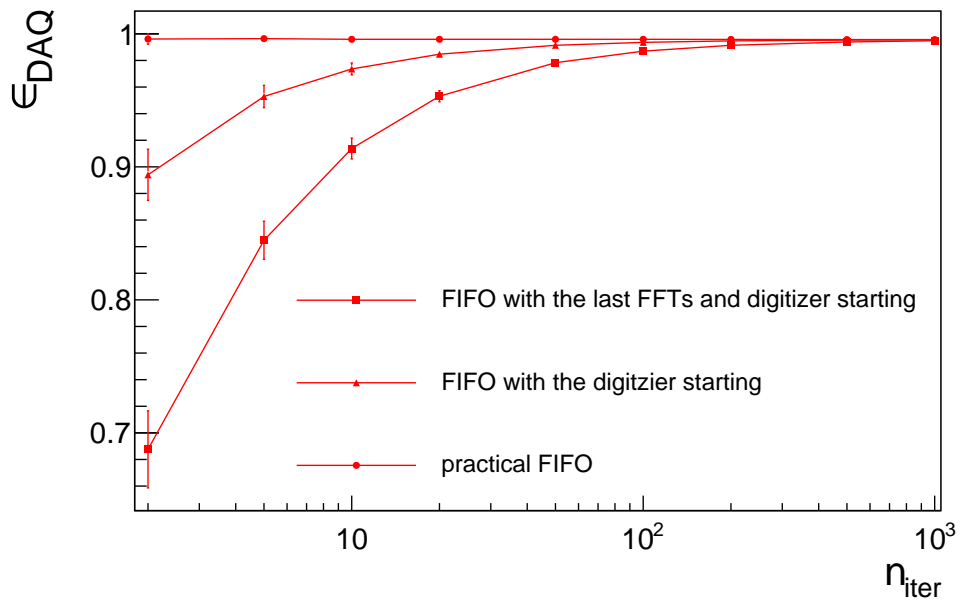


**Figure 8.** The same as Fig. 5 except for the FIFO mode only, with two parallel DAQ channels for the image rejection.

### Acknowledgments

This work is supported by the Institute for Basic Science (IBS) under Project Code No. IBS-R017-D1-2022-a00.

## References

- [1] G. 't Hooft, Phys. Rev. Lett, **37** (1976) 8; Phys. Rev. D **14** (1976) 3432; **18** (1978) 2199(E); J. H. Smith, E. M. Purcell, and N. F. Ramsey, Phys. Rev. **108** (1957) 120; W. B. Dress, P. D. Miller, J. M. Pendlebury, P. Perrin, and N. F. Ramsey, Phys. Rev. D **15** (1977) 9; I. S. Altarev *et al.*, Nucl. Phys. **A341** (1980) 269.
- [2] R. D. Peccei and H. R. Quinn, Phys. Rev. Lett. **38** (1977) 1440.
- [3] S. Weinberg, Phys. Rev. Lett. **40** (1978) 223; F. Wilczek, Phys. Rev. Lett. **40** (1978) 279.
- [4] J. Preskill, M. B. Wise, and F. Wilczek, Phys. Lett. B **120** (1983) 127; L. F. Abbott and P. Sikivie, Phys. Lett. B **120** (1983) 133; M. Dine and W. Fischler, Phys. Lett. B **120** (1983) 137.
- [5] Fuminobu Takahashi, Wen Yin, and Alan H. Guth, Phys. Rev. D **98** (2018) 015042; Peter W. Graham and Adam Scherlis, Phys. Rev. D **98** (2018) 035017.
- [6] John Ellis and K. A. Olive, Phys. Lett. B **193** (1987) 525; Georg Raffelt and David Seckel, Phys. Rev. Lett. **60** (1988) 1793; Michael S. Turner, Phys. Rev. Lett. **60** (1988) 1797; Hans-Thomas Janka, Wolfgang Keil, Georg Raffelt, and David Seckel, Phys. Rev. Lett. **76** (1996) 2621; Wolfgang Keil, Hans-Thomas Janka, David N. Schramm, Günter Sigl, Michael S. Turner, and John Ellis, Phys. Rev. D **56** (1997) 2419.
- [7] P. A. R. Ade *et al.* (Planck Collaboration), Astron. Astrophys. **594** (2016) A13.
- [8] P. Sikivie, Phys. Rev. Lett. **51** (1983) 1415; Phys. Rev. D **32** (1985) 2988.
- [9] L. Krauss, J. Moody, F. Wilczek, and D. E. Morris, Phys. Rev. Lett. **55** (1985) 1797.
- [10] B. R. Ko *et al.*, Phys. Rev. D **94** (2016) 111702(R).
- [11] S. Ahn, S. Lee, J. Choi, B. R. Ko, and Y. K. Semertzidis, J. High Energ. Phys. **2021** (2021) 297.
- [12] <https://www.rhode-schwarz.com>.
- [13] J. Choi, S. Ahn, B. R. Ko, S. Lee, and Y. K. Semertzidis, Nucl. Instrum. Methods Phys. Res., Sect. A **1013** (2021) 165667.
- [14] R. Khatiwada *et al.* (ADMX Collaboration), [arXiv:2010.00169](https://arxiv.org/abs/2010.00169).
- [15] S. Al Kenany *et al.*, Nucl. Instrum. Methods Phys. Res., Sect. A **854** (2017) 11.
- [16] Y. K. Semertzidis *et al.*, [arXiv:1910.11591](https://arxiv.org/abs/1910.11591).
- [17] A. R. Zhitnitskii, Yad. Fiz. **31** (1980) 497 [Sov. J. Nucl. Phys. **31** (1980) 260]; M. Dine, W. Fischler, and M. Srednicki, Phys. Lett. B **140** (1981) 199.
- [18] <https://spectrum-instrumentation.com>.
- [19] M. S. Turner, Phys. Rev. D **42** (1990) 3572.
- [20] P. Sikivie, I. I. Tkachev, and Y. Wang, Phys. Rev. D **56** (1997) 1863; P. Sikivie, Phys. Lett. B **567** (2003) 1; K. Freese, P. Gondolo, H. J. Newberg, and M. Lewis, Phys. Rev. Lett. **92** (2004) 111301; K. Freese, P. Gondolo, and H. J. Newberg, Phys. Rev. D **71** (2005) 043516; L. D. Duffy and P. Sikivie, Phys. Rev. D **78** (2008) 063508.
- [21] B. M. Brubaker, L. Zhong, S. K. Lamoreaux, K. W. Lehnert, and K. A. van Bibber, Phys. Rev. D **96** (2017) 123008.
- [22] M. J. Lee, B. R. Ko, and S. Ahn, JINST **16** (2021) T11008.
- [23] R. Brun, F. Rademakers, Nucl. Instrum. Methods Phys. Res., Sect. A **389** (1997) 81.

- [24] M.M. McKerns, L. Strand, T. Sullivan, A. Fang, M.A.G. Aivazis,  
<http://arxiv.org/pdf/1202.1056>; Michael McKerns and Michael Aivazis,  
<https://uqfoundation.github.io/project/pathos>.
- [25] [https://ark.intel.com/content/www/us/en/ark/products/212325/  
intel-core-i911900k-processor-16m-cache-up-to-5-30-ghz.html](https://ark.intel.com/content/www/us/en/ark/products/212325/intel-core-i911900k-processor-16m-cache-up-to-5-30-ghz.html).
- [26] Gene M. Amdahl, AFIPS Joint Spring Conference Proceedings 30 (Atlantic City, NJ, 1967), AFIPS Press, Reston VA, pp 483-485.
- [27] R. H. Dicke, Rev. Sci. Instrum. **17** (1946) 268.
- [28] <https://polyphasemicrowave.com>.
- [29] S. Lee, S. Ahn, J. Choi, B. R. Ko, and Y. K. Semertzidis, Phys. Rev. Lett. **124** (2020) 101802.